Current closed-loop control and field orientation analysis of an induction motor in six-step operation for railway applications

Fang, Xiaochun; Tian, Zhongbei; Li, Hua; Yang, Zhongping; Lin, Fei; Hillmansen, Stuart

DOI:
10.1049/iet-pel.2018.5854

Current Closed-Loop Control and Field Orientation Analysis of an Induction Motor in Six-Step Operation for Railway Applications

Xiaochun Fang[1], Zhongbei Tian[2]*, Hua Li[3], Zhongping Yang[1], Fei Lin[1], Stuart Hillmansen[2]

[1] School of Electrical Engineering, Beijing Jiaotong University, Beijing, China
[2] Department of Electronic, Electrical and Systems Engineering, University of Birmingham, Birmingham, UK
[3] CRRC Qingdao Sifang Rolling Stock Research Institute Co. Ltd, China
*z.tian@bham.ac.uk

Abstract: In railway traction drive systems, six-step operation is widely used for motors in a flux-weakening region. Traditional vector control algorithms in six-step operation cannot work effectively due to the limitation of a single degree of freedom. This paper analyses the *dq* current coupling relationship when voltage amplitude is limited and applies a current closed-loop control strategy in six-step operation. This paper proposes a proper switching control strategy to achieve a dual-mode control for induction motors in a full-speed region. The accuracy of field orientation is affected by changes in motor parameters and plays a key role in current control precision. This paper analyses the effect of field orientation error on motor six-step operation. It is found that the proposed current closed-loop control strategy can correct the field orientation error and guarantee the motor current to track the reference precisely. A case study of a 5.5 kW experimental platform is presented to validate the control schemes.

Nomenclature

u_{sd}, u_{sq}	*d*-axis and *q*-axis stator voltage
i_{sd}, i_{sq}	*d*-axis and *q*-axis stator current
R_s	Stator resistance
L_s	Stator self-inductance
σ	Total leakage factor
ω_e	Stator angular velocity
I_{smax}	Maximum stator current vector amplitude
U_{smax}	Maximum stator voltage vector amplitude
U_{dc}	Inverter DC-link voltage
ψ_r	Rotor flux
T_e	Electromagnetic torque
T_r	Rotor time constant
L_r	Rotor self-inductance
L_m	Mutual inductance
n_p	Motor pole pairs
p	Differential operator
$i_{sd.rate}$	Rated *d*-axis current
u_{sd_fd}	Feed-forward compensatory *d*-axis voltage
u_{sq_fd}	Feed-forward compensatory *q*-axis voltage
$\boldsymbol{u_s}$	Stator voltage vector
ω_r	Rotor angular velocity
ω_{base}	Motor base angular velocity
i_s	Stator current vector amplitude
δ	Field orientation angle
$*$	Subscript denotes instruction value
^	Subscript denotes estimated value

1. Introduction

Vector control has been widely used in railway induction motor (IM) control, where torque and flux linkage are controlled independently by field orientation [1, 2]. Due to the voltage limitation of the inverter DC-link, IMs require flux-weakening control to extend the operating speed. In railway traction drive systems, the inverter generally enters six-step operations to utilize DC-link voltage when the motor is in the flux-weakening region [3-5]. Compared with the linear region of the space vector pulse width modulation (SVPWM), the inverter output fundamental voltage amplitude is improved by 10.26% in six-step operations with consequent improvement of the output torque and working area. Six-step operations also reduce the switching frequency and, hence, inverter power loss. Thus, six-step operations are helpful to reduce inverter size and weight.

There are four main types of IM flux-weakening control [6, 7]. 1) Calculating the rotor flux instruction inversely proportional to motor speed. This method is simple, but it is difficult to provide the optimal flux linkage reference [8, 9]. 2) Calculating excitation current instruction according to a motor model. The control performance is sensitive to changes in motor parameters [10, 11]. 3) The excitation current and torque current reference can be obtained from a lookup table, but this method lacks portability [12]. 4) The difference between maximum inverter output voltage and motor stator voltage is used as the input of the voltage regulator to adjust excitation current [13-15]. This method does not depend on motor parameters and improves the robustness of flux-weakening control. The conventional flux-weakening control methods mentioned above require independent control of *dq* current. Thus, a threshold should be kept between the usable voltage and the maximum inverter output voltage, to guarantee the dynamic response of current regulators. Siebel et al. [16] stated that a threshold of 3% maximum inverter output voltage is required, while Sahoo and colleagues [17, 18] proposed a maximum voltage usage ratio of 96.34%. In six-step operation, motor voltage amplitude is fixed, and the voltage usage ratio is 100%. There is only one controllable degree of freedom, which is the voltage angle. Current regulators for conventional flux-weakening control will saturate in a six-step operation, which leads to these methods being disabled.

To achieve IM flux-weakening control in six-step operation, current open-loop control is used instead of double current regulators in six-step operation [19, 20]. The current response ability of this method is limited. Four PI controllers

are involved in switching the control strategies before and after six-step operation, which is too complicated to achieve. Horie et al. and Ando et al. [21, 22] abandoned the excitation current regulator in six-step operation, so that only the torque current is controlled by a closed loop. The excitation current is regulated by the error of the *q*-axis current in the work of Sahoo and Bhattacharya [23], thus torque current and excitation current closed-loop control is achieved near six-step operation. However, the coupling regulation relationship between excitation current and torque current has not been presented clearly. In addition, the motor cannot operate continuously in six-step mode under constant load conditions [23]. Which lead to extra switching action of power electronic devices than in stable six-step operation. The *dq* current coupling effect of PMSM in a high-speed region was used by Fang et al. [24]. Flux-weakening control is achieved by a single *d*-axis current regulator. The precise current trajectory tracking is achieved in a *dq* current coordinate system, and maximum inverter output voltage can be used stably and continuously. Fang et al. [24] achieved current closed-loop control with maximum inverter voltage usage for PMSM, but it was in SVPWM linear region and without consideration of inverter switching frequency. Sahoo and Bhattacharya [23] tried to achieve current closed-loop control with maximum inverter voltage usage for IM, but just near six-step operation was realized.

High-performance motor control requires proper current control strategies and precise field orientation. During train operation, motor parameters can change because of temperature, flux saturation, skin effect, etc. As a result, the motor field orientation will be inaccurate. This will reduce the motor control performance, causing inaccuracy of output torque and even transient oscillation [25]. Motor parameters can be observed by signal injection, state observer, model reference adaptive techniques, artificial intelligence, etc. [26, 27]. However, not all of them can be used for precise rotor field orientation. Yoo et al. [28] derived a compensated value for the rotor time constant based on a motor model, but neglected the change in inductor parameters. Maiti et al. [29] used reactive power to identify rotor resistance, but the results were affected by inductor parameters and PWM dead-time. Junfeng et al. [30] revised the field orientation by observing the torque difference in different coordinate systems. This method is simple but has to use inductor parameters to observe torque. The field orientation correction strategies mentioned above are used when the inverter output voltage usage ratio is lower than 100%, which is not suitable for six-step operation.

This paper studies flux-weakening control in six-step operation for IMs in railway traction systems. Section 2 addresses the IM coupling effect of excitation and torque in a high-speed region. Based on the coupling effect, a current closed-loop flux-weakening control to realize fast torque control in six-step operation is proposed. This section also presents the proper switching principle to guarantee that the motor can work continuously in six-step operation without unreasonable switching between PWM mode. Section 3 analyses the effect of inaccurate field orientation on the motor output torque, flux linkage and *dq* current in six-step operation. In addition, field orientation self-correction by the proposed control strategy is analysed. Section 4 verifies the proposed control strategy based on the experiment case study. Finally, Section 5 provides a conclusion.

2. Flux-weakening control in six-step operation

2.1. Coupling relationship of dq current

In a synchronous rotating coordinate system, according to rotor field orientation, the steady-state formulas of IM stator voltage are given by equation (1).

$$\begin{cases} u_{sd} = R_s i_{sd} - \omega_e \sigma L_s i_{sq} \\ u_{sq} = R_s i_{sq} + \omega_e L_s i_{sd} \end{cases} \tag{1}$$

By transforming the *q*-axis voltage formula in equation (1), the *q*-axis current can be obtained using equation (2).

$$i_{sq} = \frac{u_{sq}}{R_s} - \frac{\omega_e L_s i_{sd}}{R_s} \tag{2}$$

It can be observed from equation (2) that, at a non-zero speed, if u_{sq} is fixed, the motor *dq* current has a linear relationship. The linear relationship is sound in small signal range where L_s and R_s can be assumed to be constant. This linear relationship represents the *dq* current coupling effect. The coupling coefficient ($\omega_e L_s / R_s$) increases with an increase in stator frequency, which means the coupling effect is stronger with an increase in stator frequency.

The motor operation is limited by stator current and voltage, as shown in equation (3). I_{smax} depends on invertor and motor rated current, and U_{smax} depends on invertor DC-link voltage and modulation strategies.

$$\begin{cases} u_{sq}^2 + u_{sd}^2 \le U_{s\max}^2 \\ i_{sq}^2 + i_{sd}^2 \le I_{s\max}^2 \end{cases} \tag{3}$$

When the stator frequency is low, U_{smax} is much higher than motor back EMF. The u_{sq} in equation (2) has enough range to be adjusted, and the coupling effect is easy to limit. Thus, double current regulators can achieve instantaneous current control. Fig. 1 shows a typical double current regulator control scheme for an induction traction motor below base frequency. To improve the response speed of motor current, feed-forward compensation is used to achieve *dq* current decoupling.

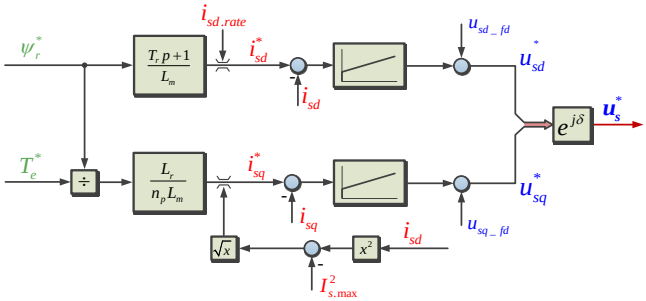

Fig. 1. *Double current regulator vector control*

With an increase in motor speed, flux-weakening control is required to reduce the back EMF to extend the operation region. The traditional flux-weakening control method has a voltage threshold to guarantee independent control of *dq* current regulators and to avoid saturation. This type of method cannot fully use the invertor voltage and achieve six-step operation. When the traction system is in six-

step operation, the inverter exports the maximal output voltage. The relationship of motor *dq* voltage is fixed as shown in equation (4). The control system has only one degree of freedom, which is the voltage phase angle. The *dq* current cannot be decoupled and controlled independently.

$$u_{sq} = \sqrt{U_{s\max}^2 - u_{sd}^2} \tag{4}$$

2.2. Current closed-loop control in six-step operation

To achieve current closed-loop control in six-step operation, this paper utilizes the strong coupling effect of *dq* current in equation (2). Adjustment of the *dq* voltage instruction is shown in Part 1 of Fig. 2, and the overall control scheme is shown in Fig. 2. Only the *d*-axis current regulator remains to adjust voltage instructions in six-step operation. Motor excitation and torque control are completed by a single *d*-axis current regulator. The *q*-axis voltage instruction is not obtained from the *q*-axis current regulator but is calculated from equation (5) using inverter maximal output voltage and *d*-axis voltage instruction. The instantaneous sampled and updated U_{dc} is used to calculate U_{smax}. Thus, the impact of U_{dc} fluctuation on the six-step operations is eliminated. To guarantee the motor response speed in six-step operation, the *d*-axis voltage instruction is calculated by the *d*-axis voltage feed-forward part u_{sd_fd} and the *d*-axis current PI controller. In this way, the limitation of a single degree of freedom in six-step operation is fulfilled, and current closed-loop control is achieved.

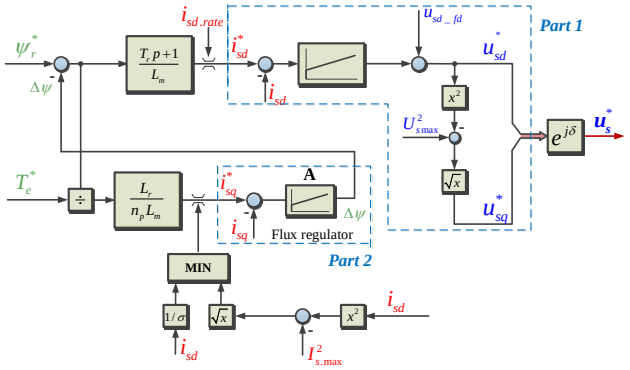

Fig. 2. *Current control scheme in six-step operation*

$$\begin{cases} u_{sq}^* = \sqrt{U_{s\max}^2 - u_{sd}^{*\,2}} \\ U_{s\max} = 2u_{dc}/\pi \\ u_{sd}^* = u_{sd\_fd} + PI\_out\_i_{sd} \end{cases} \tag{5}$$

To fulfil the current limitation of having motor and output torque as high as possible, the *dq* current should be limited as shown in equation (6). Detailed analysis can be found in the work of Kim and Sul [10].

$$\begin{cases} i_{sd\_\lim} = i_{sd\_rate} \\ i_{sq\_\lim} = \min(\sqrt{I_{s\max}^2 - i_{sd}^2}, i_{sd}^*/\sigma) \end{cases} \tag{6}$$

In addition, to improve the response ability of the *q*-axis current, the *q*-axis current error is used to adjust the rotor flux linkage reference ψ_r^* by PI regulator A, which is shown in Part 2 of Fig. 2.

2.3. Full-speed region dual-mode control and switching strategies

According to the traditional double current regulator vector control in Fig. 1 and the current closed-loop control in six-step operation in Fig. 2, this paper proposes a dual-mode control scheme for traction IM, which is suitable to operate with a multi-mode hybrid PWM strategy, as shown in Fig. 3.

When IM is in the constant torque region, and the speed is lower than ω_{base}, the motor voltage has not reached the maximum voltage limit. The motor should only meet the current constraint, and the traditional double current regulator vector control is used. When the motor speed increases and enters a flux-weakening region, the six-step operation current closed-loop control is applied to utilize the maximum voltage.

To achieve dual-mode control in a full-speed region, two control schemes need to be switched to each other online. When the control scheme in Fig. 1 is applied, the relationship among u_{sq}^*, U_{smax} and u_{sd}^* is given by equation (7).

$$u_{sq}^* < \sqrt{U_{s\max}^2 - u_{sd}^{*\,2}} \tag{7}$$

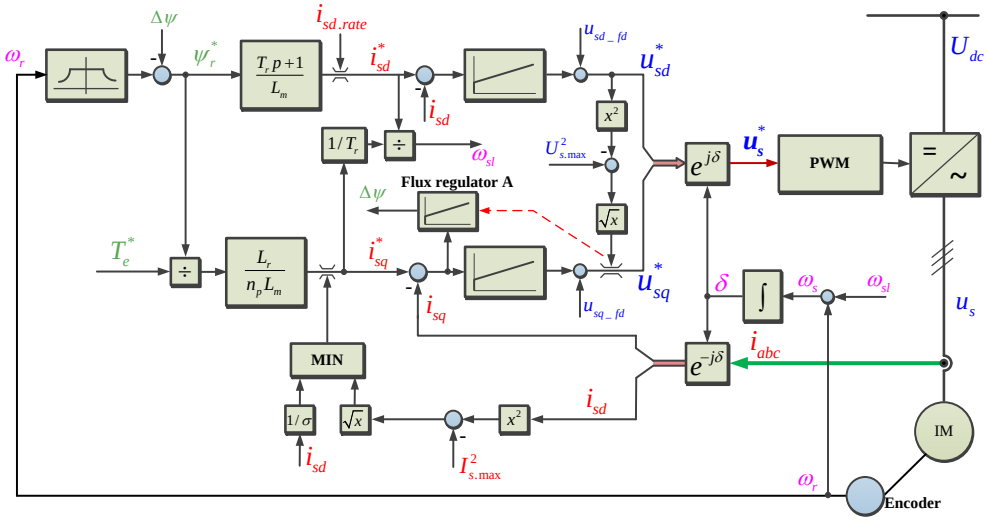

Fig. 3. *Dual-mode control scheme*

With an increase in the motor speed or the load, u_{sq}^* moves closer to $\sqrt{U_{s\max}^2 - u_{sd}^2}$. When:

$$u_{sq}^* \geq \sqrt{U_{s\max}^2 - u_{sd}^{*2}} \tag{8}$$

the control scheme in Fig. 1 is no longer applicable, and the six-step control scheme in Fig. 2 needs to be used. Thus, equation (8) is the entry condition for six-step operation.

When the motor enters six-step operation, u_{sq}^* is fixed at $\sqrt{U_{smax}^2 - u_{sd}^2}$. Equation (8) is always met, so u_{sq}^* cannot be used as the flag to quit six-step operation. In six-step operation, another *q*-axis voltage instruction can be exported from the *q*-axis current regulator in Fig. 1, which is defined as u_{sq1}^* and is not used to control the motor. u_{sq1}^* is different from u_{sq}^* calculated by equation (5). Putting u_{sq1}^* into equation (7) determines whether quitting six-step operation is also not applicable. When the six-step control scheme in Fig. 2 is used, i_q can track i_q^* rapidly, and the motor back EMF is limited due to flux-weakening control. Thus, u_{sq1}^* can satisfy equation (7) and lead to unreasonable switching off of six-step operation. The overall system is operated close to six-step operation in steady state and switched to six-step operation temporarily when the system instruction changes rapidly. This causes too high a system switching frequency in the high-speed region, and the DC-link voltage is not fully used.

To solve the problems above, d-axis current is used as the criteria of quitting six-step operation. As shown in Fig. 4, when the motor speed or the load reduces, the motor operation point moves to the right side of the curve $i_{sd} = i_{sd.rate}$ and should quit the six-step operation. Thus, the criteria of quitting six-step operation can be obtained by relation between i_{sd} and $i_{sd.rate}$ as shown in equation (9). When the d-axis current is above $i_{sd.rate}$, the six-step flux-weakening control is switched off, and the conventional double current regulator vector control in Fig. 1 is recovered. In the meantime, the adjustment of flux linkage by the *q*-axis is forbidden. The integrator item of the regulator is cleared to avoid impact on the control. The holistic criterion for switching six-step operation is shown in Fig. 5.

$$i_{sd} > i_{sd.rate} \tag{9}$$

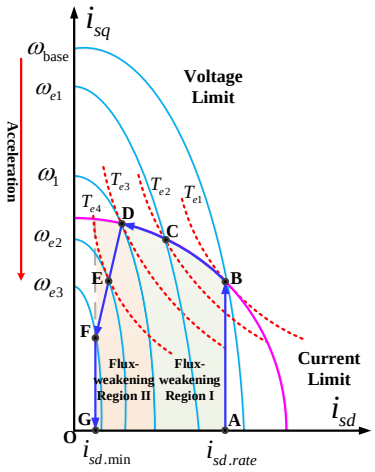

Fig. 4. *Working areas of IM*

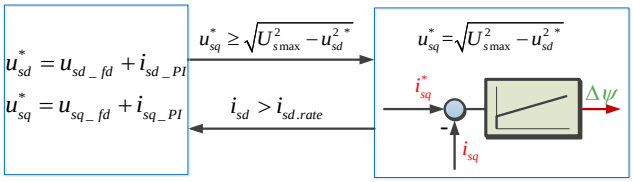

Fig. 5. *Switching control strategy*

3. Field orientation error effect analysis and self-correction

In an indirect field-oriented vector control system, the field location is calculated by integrating the sum of rotor frequency and slip frequency, as in equation (10).

$$\begin{cases} \omega_e = \omega_r + \dfrac{i_{sq}}{T_r i_{sd}} \\ \delta = \int \omega_e dt \end{cases} \tag{10}$$

In practical operation, a change in motor parameters and control delay can lead to a change in the actual rotor time constant T_r. A difference between T_r and estimated rotor time constant $\hat{T}_r$ in the controller can lead to an error in stator frequency calculation and inaccuracy in the field orientation angle δ. Regarding motor control systems with a speed sensor, the actual slip frequency equals the given slip frequency when the speed measurement is accurate.

$$\frac{i_{sq}}{T_r i_{sd}} = \frac{i_{sq}^*}{\hat{T}_r i_{sd}^*} \tag{11}$$

In medium- and low-speed regions, due to PI control of double current regulators, no matter whether the field orientation is accurate or not, the amplitude of actual stator current is consistent with the reference current. When field orientation is inaccurate, there is an error between the actual *dq* current and instructions. In six-step operation, no matter whether the field orientation is accurate or not, the amplitude of the stator voltage remains the same. When field orientation is inaccurate, the actual angle of the motor voltage is changed, which leads to an error between the actual *dq* voltage and instructions, as shown in Fig. 6.

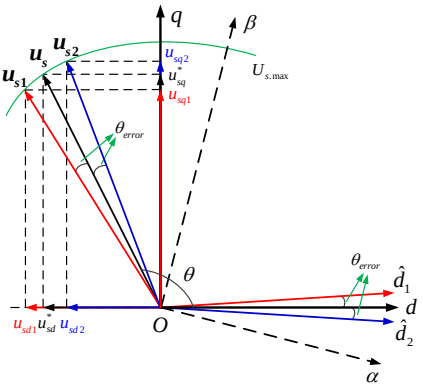

Fig. 6. *Change in voltage vector angle when six-step operation field orientation is inaccurate*

From Fig. 6, when field orientation is inaccurate, the error of the stator voltage angle is given by equation (12).

$$\theta_{error} = arc\tan\left(\frac{u_{sq}}{u_{sd}}\right) - arc\tan\left(\frac{u_{sq}^*}{u_{sd}^*}\right) \tag{12}$$

In a flux-weakening region, the stator frequency is high. Thus, the voltage of stator resistance can be neglected, and the steady-state voltage in equation (1) can be simplified as equation (13).

$$\begin{cases} u_{sd} = -\omega_e \sigma L_s i_{sq} \\ u_{sq} = \omega_e L_s i_{sd} \end{cases} \tag{13}$$

By combining equations (11) and (13) into equation (12), equation (14) is obtained.

$$\theta_{error} = arc\tan\left(\frac{1}{T_r/\hat{T}_r}\frac{1}{\sigma i_{sq}^*/i_{sd}^*}\right) - arc\tan\left(\frac{1}{\sigma i_{sq}^*/i_{sd}^*}\right) \tag{14}$$

According to equation (14), the relationship between voltage angle error and rotor time constant error can be obtained, as shown in Fig. 7. With an increasing error between the estimated rotor time constant $\hat{T}_r$ and the actual time constant T_r, the field orientation angle error increases. When the rotor time constant error is fixed, with an increase in $|i_{sq}^*/i_{sd}^*|$ which represents load, the field orientation angle error increases.

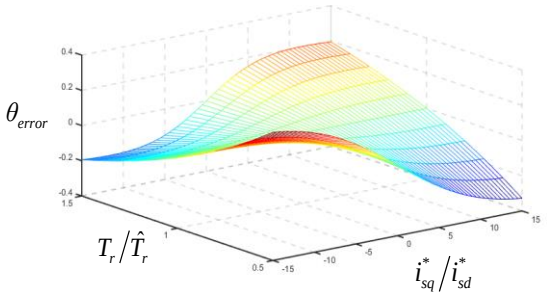

Fig. 7. *Relationship of* $\boldsymbol{\theta_{error}}$ *to rotor time constant error and load*

The relationship between *dq* voltage and angle error is denoted in equation (15).

$$\begin{cases} u_{sd} = U_{s.max}\cos(\theta + \theta_{error}) \\ u_{sq} = \sqrt{U_{s\,max}^2 - u_{sd}^2} \end{cases} \tag{15}$$

Based on equation (15), when the stator angle is ahead, $|u_{sd}|$ is higher than $|u_{sd}^*|$, and u_{sq} is lower than u_{sq}^*. On the contrary, u_{sq} is higher and $|u_{sd}|$ is lower. By combining equations (13) and (15), the actual motor *dq* current is given by equation (16).

$$\begin{cases} i_{sd} = \dfrac{\sqrt{U_{s\,max}^2 - u_{sd}^2}}{\omega_e L_s} \\ i_{sq} = -\dfrac{U_{s.max}\cos(\theta + \theta_{error})}{\omega_e \sigma L_s} \end{cases} \tag{16}$$

According to equation (16), if the motor parameters in Table 1 are applied, the actual *dq* current when θ_{error} is within [−7π/18 and 7π/18] is shown in Fig. 8.

From Fig. 8, when the field orientation angle δ is ahead ($\theta_{error} > 0$), the actual *d*-axis current i_{sd} is lower than i_{sd}^*, and the *q*-axis current i_{sq} is higher than i_{sq}^*. When six-step operation closed-loop control is used, the output of the PI controller A in Fig. 2 decreases, which leads to an increase in the rotor flux linkage instruction ψ_r^*. The increase of ψ_r^* improves the excitation current instruction i_{sd}^*. The increase of i_{sd}^* leads to a decrease in $|u_{sd}|$ and an increase in u_{sq}. The stator voltage vector moves along the voltage-limit circle clockwise, which reduces the voltage vector angle error, as $\boldsymbol{u_{s1}}$ shown in Fig. 9.

When the field orientation angle lags, i_{sd} is higher than i_{sd}^*, and i_{sq} is lower than i_{sq}^*. The variables in six-step operation closed-loop control change in the opposite way to when the field orientation angle is ahead. The stator voltage vector moves the along the voltage-limit circle anticlockwise, which reduces the voltage vector angle error, as $\boldsymbol{u_{s2}}$ shown in Fig. 9.

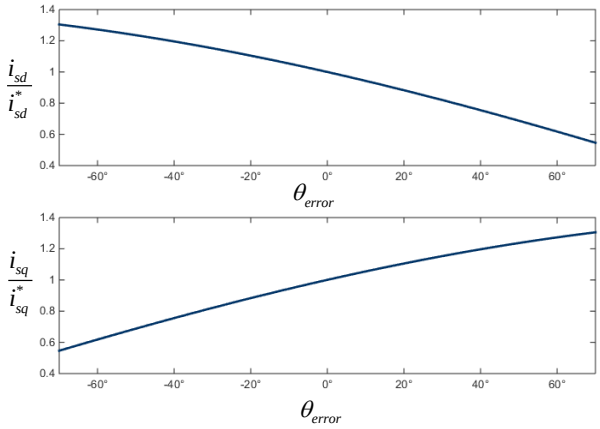

Fig. 8. *Relationship between dq current and* θ_{error}

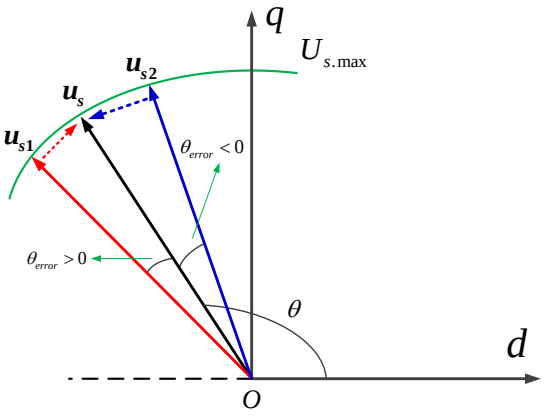

Fig. 9. *Voltage variation in field orientation correction*

The analysis above denotes that, using six-step operation current closed-loop control, the system can be adjusted automatically when field orientation is inaccurate due to rotor time constant changes. Thus, the accuracy of the motor voltage vector angle in six-step operation is guaranteed.

4. Analysis of experimental results

The experimental platform is shown in Fig. 10, which consists of a traction IM, a load motor, two three-phase

converters and two control systems. A TMS320F28335 floating point digital signal processor is used to control the traction IM. The load motor is controlled by a Myway platform. The detailed experimental motor parameters are shown in Table 1.

Table 1 Parameters of the experimental motor platform

Parameter	Value
Stator resistance/Ω	1.9
Rotor resistance/Ω	1.09
Stator leakage inductance/H	0.01629
Rotor leakage inductance/H	0.01629
Mutual inductance/H	0.430875
Pole pairs	2
Rated power/kW	5.5
Full load torque/Nm	35
Rotating speed/(r/min)	1450
Rated current/A	11.9
DC bus voltage/V	513

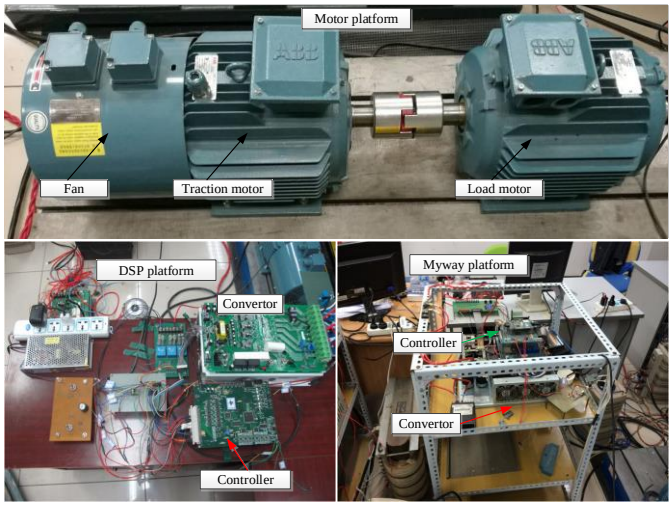

Fig. 10. *Experimental platform*

As shown in the Fig. 3 , the calculation of i_{sd}^* and i_{sq}^* refer to L_r and L_m. Although there exists variation of leakage inductance, it is very small compared to variation of excitation induction. Thus, the accuracy of i_{sd}^* and i_{sq}^* is mainly affected by the change of L_m. L_m is mainly influenced by field current and can be corrected by offline measurement. For the experimental motor used in this paper, the relationship between L_m and field current is shown in Fig. 11.

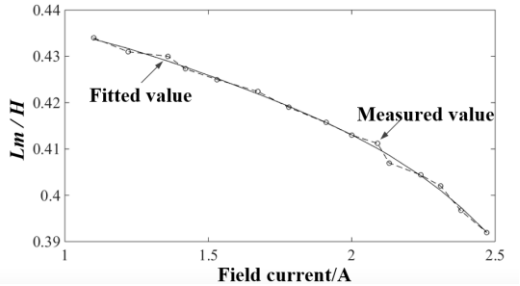

Fig. 11. L_m *against field current*

To simulate the traction motor operation environment, this paper applies multi-mode PWM and limits the switching frequency. Since the range of experimental motor speed regulation is relatively narrow, and the power and voltage ranking is relatively low, this paper simplifies the multi-mode PWM, as shown in Fig. 12(a). The full-speed region uses the asynchronous SVPWM and a synchronous 11-pulse Basic Bus Clamping Strategy (BBCS) SVPWM [31]. Finally, six-step operation is achieved by 11-pulse SVPWM overmodulation. The PWM results are shown in Fig. 12(b), (c) and (d).

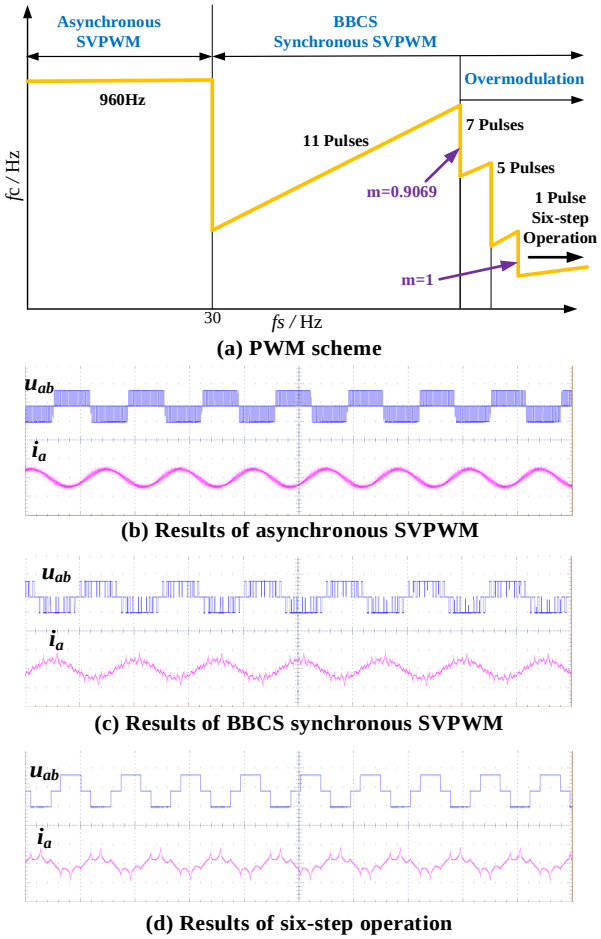

Fig. 12. *The PWM strategy of the platform*

4.1. Full-speed region dual-mode control and switching strategies

Fig. 13 shows the experimental results when the motor accelerates to 1500 r/min then decelerates. Fig. 13(a) shows *dq* current and phase voltage amplitude during this process. It can be found that the *q*-axis current remains the same after the motor enters six-step operation, and there is no impact on *dq* current when switching control strategies. To meet the maximum voltage limit in six-step operation, regulator A in Fig. 2 is used to reduce *d*-axis current. From Fig. 13(a), it can be seen that using the proposed closed-loop control in six-step operation can make the phase voltage amplitude the same with the maximum output voltage of inverter U_{smax}. The motor works stably in six-step operation. Fig. 13(b) and Fig. 13(c) shows the phase current and line voltage waveforms around the switching point of six-step operation. The motor enters and quits six-step operation smoothly.

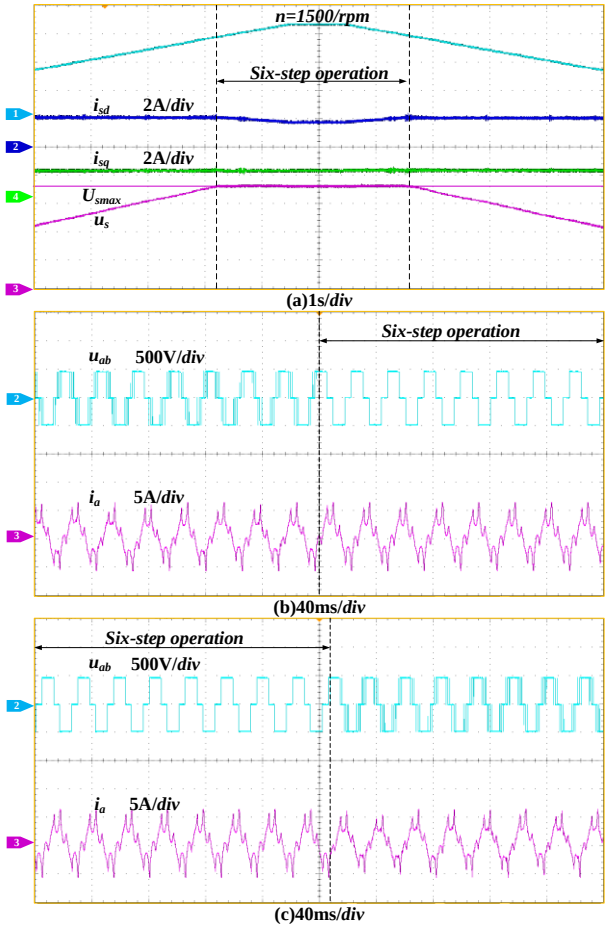

Fig. 13. *Experimental results for dual-mode control*

4.2. Current response experiment in six-step operation

To validate the current response ability in six-step operation, a load experiment was carried out. The load motor controls the speed, while the experiment motor controls the torque.

Fig. 14 shows the *dq* current and phase current response when the motor is at 1300 r/min and the torque current instruction is changed suddenly. The *q*-axis current instruction is changed from 3 A to 1 A, and then increases to 2 A. It was found that the dynamic response is good when the *dq* current instruction is changed suddenly. The *dq* current can track the instructions rapidly, and phase current can respond rapidly to guarantee the accurate output of motor torque.

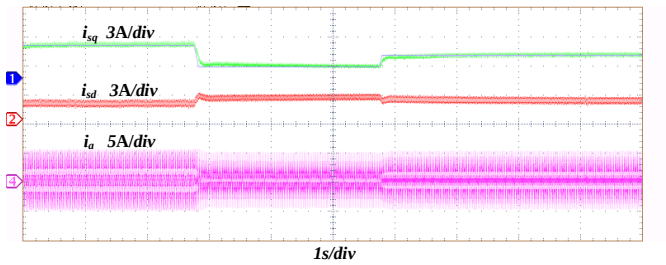

Fig. 14. *Current response with instruction changes*

4.3. Field orientation self-correction experiment

The traction motor torque instruction is 6 Nm, and the load motor speed is 1200 r/min. The proposed six-step operation current closed-loop control strategy is applied to the traction IM. The traction motor works stably in six-step operation. The estimated rotor time constant $\hat{T}_r$ in the DSP controller is changed at t_1 and t_2; the experimental results are shown in Fig. 15.

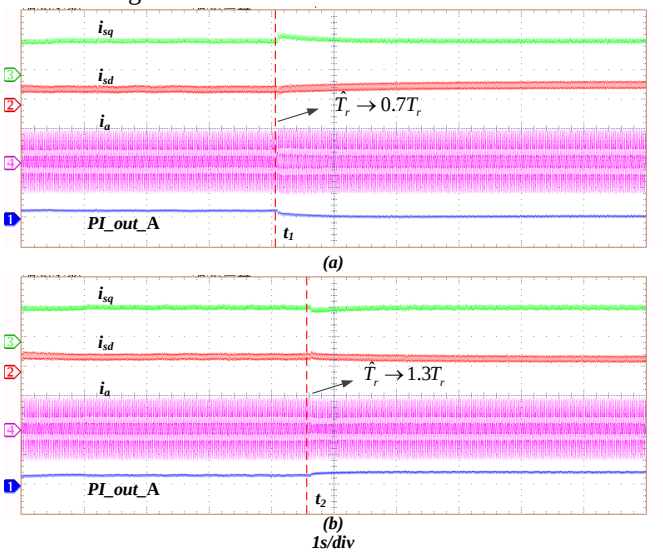

Fig. 15. *Motor response when rotor time constant is changed*

Fig. 15(a) shows the *dq* current and phase current response when $\hat{T}_r$ is changed to $0.7T_r$ at t_1. It was found that, at the instant $\hat{T}_r$ changes, the field orientation angle is ahead. This leads to the voltage angle being ahead, higher *q*-axis current i_{sq}, lower *d*-axis current i_{sd}, and a slight increase in phase current i_a. Thus, the output of regulator A PI_out_A decreases, which leads to an increase in the *d*-axis current instruction i_{sd}^*. As a result, $|u_{sd}|$ decreases and u_{sq} increases. The voltage vector angle rotates clockwise, which reduces the error of the voltage vector angle. Thus, the *q*-axis current can track the instruction value rapidly, and phase current amplitude becomes the original value. Fig. 15(b) shows *dq* current and phase current when $\hat{T}_r$ is changed to $1.3T_r$ at t_2. The experimental results are the opposite when $\hat{T}_r$ decreases. PI_out_A increases, which leads to a decrease in voltage vector error. The *q*-axis current tracks the instruction value rapidly.

The experimental results are consistent with the theoretical analysis. Using the proposed current closed-loop control, inaccurate field orientation due to changes in motor parameter can be corrected rapidly, to guarantee that the motor current tracks the instruction. Thus, the motor output torque will be as expected.

5. Conclusion

Traction IMs in railway applications should employ six-step operation in high-speed regions. There is only one degree of freedom in such a system, so it is difficult to achieve current closed-loop control using conventional flux-weakening control with double current regulators. This paper analyses the coupling relationship between *dq* current based on IM voltage equation when the motor stator voltage is limited. Using this relationship, a flux-weakening scheme with fast current response is applied, where *dq* voltage

instructions are adjusted by a single *d*-axis current regulator. Based on the proposed control scheme, full-speed dual-mode control of the IM is achieved. Switching principle between six-step and PWM modes is analysed. Smooth switching between the two control modes is achieved by proper switching control. The IM can work stably in six-step operation without unreasonable and repeated switching between PWM modes and accomplish rapid current closed-loop control.

Changes in motor parameters can cause inaccuracy of field orientation. This paper analyses the influence of inaccurate field orientation on IM six-step operation. 1) When the rotor time constant error is fixed, an increase in load leads to an increase in field orientation angle error. 2) When the field orientation angle is ahead, the actual *d*-axis current is lower than the instruction, and the actual *q*-axis current is higher than the instruction, and vice versa. Moreover, it is found that the proposed six-step operation current closed-loop control strategy can achieve accurate tracking of current instruction by self-correction of the field orientation.

The case study presents validation of the proposed control scheme and analysis on a 5.5 kW experimental platform. This approach can be also employed in other scenarios using IM in six-step operation.

6. Acknowledgments

This research is supported by the research and development plan of the Ministry of Science and Technology 13th Five-Year Plan (2016YFB1200506-18).

7. References

[1] L. Guo, Z. Yang, F. Lin, and X. Tu, "Weighted torque current control for high speed train with dual induction motors fed by a single inverter," in *IECON 2015 - 41st Annual Conference of the IEEE Industrial Electronics Society*, 2015, pp. 002723-002728.

[2] D. Perna and A. D. Pizzo, "An assisted speed-sensorless control of induction motor drives for railways applications," in *2016 International Conference on Electrical Systems for Aircraft, Railway, Ship Propulsion and Road Vehicles & International Transportation Electrification Conference (ESARS-ITEC)*, 2016, pp. 1-7.

[3] J. Holtz and N. Oikonomou, "Fast Dynamic Control of Medium Voltage Drives Operating at Very Low Switching Frequency—An Overview," *IEEE Transactions on Industrial Electronics*, vol. 55, no. 3, pp. 1005-1013, 2008.

[4] X. Fang, F. Lin, and Z. Yang, "An Improved Central 60 Synchronous Modulation for High Transient Performance with PMSM Stator Flux Control Used in Urban Rail Transit Systems," *Journal of Power Electronics*, vol. 16, no. 2, pp. 542-552, 2016.

[5] C. Wang, K. Wang, and X. You, "Research on Synchronized SVPWM Strategies Under Low Switching Frequency for Six-Phase VSI-Fed Asymmetrical Dual Stator Induction Machine," *IEEE Transactions on Industrial Electronics*, vol. 63, no. 11, pp. 6767-6776, 2016.

[6] P. Y. Lin and Y. S. Lai, "Novel Voltage Trajectory Control for Field-Weakening Operation of Induction Motor Drives," *IEEE Transactions on Industry Applications*, vol. 47, no. 1, pp. 122-127, 2011.

[7] M. Mengoni, L. Zarri, A. Tani, G. Serra, and D. Casadei, "A Comparison of Four Robust Control Schemes for Field-Weakening Operation of Induction Motors," *IEEE Transactions on Power Electronics*, vol. 27, no. 1, pp. 307-320, 2012.

[8] X. Xu and D. W. Novotny, "Selection of the flux reference for induction machine drives in the field weakening region," *IEEE transactions on industry applications*, vol. 28, no. 6, pp. 1353-1358, 1992.

[9] M.-H. Shin, D.-S. Hyun, and S.-B. Cho, "Maximum torque control of stator-flux-oriented induction machine drive in the field-weakening region," *IEEE Transactions on Industry Applications*, vol. 38, no. 1, pp. 117-122, 2002.

[10] S.-H. Kim and S.-K. Sul, "Maximum torque control of an induction machine in the field weakening region," *IEEE Transactions on Industry Applications*, vol. 31, no. 4, pp. 787-794, 1995.

[11] F. Briz, A. Diez, M. W. Degner, and R. D. Lorenz, "Current and flux regulation in field-weakening operation [of induction motors]," *IEEE Transactions on Industry Applications*, vol. 37, no. 1, pp. 42-50, 2001.

[12] G. Gallegos-López, F. S. Gunawan, and J. E. Walters, "Current control of induction machines in the field-weakened region," *IEEE Transactions on Industry Applications*, vol. 43, no. 4, pp. 981-989, 2007.

[13] S.-H. Kim and S.-K. Sul, "Voltage control strategy for maximum torque operation of an induction machine in the field-weakening region," *IEEE Transactions on Industrial Electronics*, vol. 44, no. 4, pp. 512-518, 1997.

[14] L. Harnefors, K. Pietilainen, and L. Gertmar, "Torque-maximizing field-weakening control: design, analysis, and parameter selection," *IEEE Transactions on Industrial Electronics*, vol. 48, no. 1, pp. 161-168, 2001.

[15] M. Mengoni, L. Zarri, A. Tani, G. Serra, and D. Casadei, "Stator flux vector control of induction motor drive in the field weakening region," *IEEE Transactions on Power Electronics*, vol. 23, no. 2, pp. 941-949, 2008.

[16] B. J. Seibel, T. M. Rowan, and R. J. Kerkman, "Field-oriented control of an induction machine in the field-weakening region with DC-link and load disturbance rejection," *IEEE Transactions on Industry Applications*, vol. 33, no. 6, pp. 1578-1584, 1997.

[17] S. K. Sahoo, T. Bhattacharya, and M. Aravind, "A synchronized sinusoidal PWM based rotor flux oriented controlled induction motor drive for traction application," in *Applied Power Electronics Conference and Exposition (APEC), 2013 Twenty-Eighth Annual IEEE*, 2013, pp. 797-804: IEEE.

[18] S. K. Sahoo and T. Bhattacharya, "Rotor flux-oriented control of induction motor with synchronized sinusoidal PWM for traction application," *IEEE Transactions on Power Electronics*, vol. 31, no. 6, pp. 4429-4439, 2016.

[19] I. Yasuoka, T. Henmi, Y. Nakazawa, and I. Aoyama, "Improvement of re-adhesion for commuter trains with vector control traction inverter," in *Power Conversion Conference-Nagaoka 1997., Proceedings of the*, 1997, vol. 1, pp. 51-56: IEEE.

[20] Y. Nakazawa, S. Toda, I. Yasuoka, and H. Naito, "One-pulse PWM mode vector control for traction drives," in *Power Electronics in Transportation, 1996., IEEE*, 1996, pp. 135-141: IEEE.

[21] A. Horie, T. Mizobuchi, K. Nakamura, and D. Eng, "Efficient train traction system that reduces maintenance work," *Hitachi Rev.*, vol. 48, pp. 139-143, 1999.
[22] T. Ando, T. Tanamachi, E. Toyota, K. Nakata, M. Suzuki, and K. Yasuda, "Apparatus and method for controlling induction motor," ed: Google Patents, 2000.
[23] S. K. Sahoo and T. Bhattacharya, "Field Weakening Strategy for a Vector-Controlled Induction Motor Drive Near the Six-Step Mode of Operation," *IEEE Transactions on Power Electronics*, vol. 31, no. 4, pp. 3043-3051, 2016.
[24] X. Fang, F. Lin, and Z. Yang, "A modified flux-weakening control method of PMSM based on the dq current cross-coupling effect," in *Transportation Electrification Asia-Pacific (ITEC Asia-Pacific), 2014 IEEE Conference and Expo*, 2014, pp. 1-6: IEEE.
[25] C. Mastorocostas, I. Kioskeridis, and N. Margaris, "Thermal and slip effects on rotor time constant in vector controlled induction motor drives," *IEEE Transactions on power electronics*, vol. 21, no. 2, pp. 495-504, 2006.
[26] H. A. Toliyat, E. Levi, and M. Raina, "A review of RFO induction motor parameter estimation techniques," *IEEE transactions on Energy conversion*, vol. 18, no. 2, pp. 271-283, 2003.
[27] M. S. Zaky, M. M. Khater, S. S. Shokralla, and H. A. Yasin, "Wide-speed-range estimation with online parameter identification schemes of sensorless induction motor drives," *IEEE Transactions on Industrial Electronics*, vol. 56, no. 5, pp. 1699-1707, 2009.
[28] A. Yoo, C. Hong, and J.-I. Ha, "On-line rotor time constant estimation for indirect field oriented induction machine," in *Energy Conversion Congress and Exposition (ECCE), 2013 IEEE*, 2013, pp. 3860-3865: IEEE.
[29] S. Maiti, C. Chakraborty, Y. Hori, and M. C. Ta, "Model reference adaptive controller-based rotor resistance and speed estimation techniques for vector controlled induction motor drive utilizing reactive power," *IEEE Transactions on Industrial Electronics*, vol. 55, no. 2, pp. 594-601, 2008.
[30] Y. Junfeng, W. XiaoLin, D. Zhiquan, and Q. Liao, "Slip frequency correction based on torque observer for induction machine indirect vector control system," in *2014 IEEE Conference and Expo Transportation Electrification Asia-Pacific (ITEC Asia-Pacific)*, 2014, pp. 1-4.
[31] G. Narayanan and V. Ranganathan, "Two novel synchronized bus-clamping PWM strategies based on space vector approach for high power drives," *IEEE Transactions on Power Electronics*, vol. 17, no. 1, pp. 84-93, 2002.